Kinetics of the Reaction between OH and HO_2 on the Singlet Potential Energy Surface

Carlos Gonzalez, John Theisen, Ling Zhu, H. Bernhard Schlegel, William L. Hase,*

Department of Chemistry, Wayne State University, Detroit, Michigan 48202

and E. W. Kaiser

Chemistry Department, Research Staff, Ford Motor Company, Dearborn, Michigan 48121-2053
(Received: January 22, 1991; In Final Form: April 8, 1991)

Electronic structure calculations at the HF, MP2, and MP4 levels of theory, with the 6-31G** basis set, are reported for stationary points on the OH + HO_2 singlet potential energy surface. Two particularly important stationary points are the trioxide (H_2O_3) global minimum and the reaction transition state for $O_2(^1\Delta)$ + H_2O formation. For the latter, the MP4 0 K barrier height is 15.2 kcal/mol. Thus, the formation of $O_2(^1\Delta)$ and H_2O is predicted to be unimportant, except at highly elevated temperatures. MP2 vibrational frequencies calculated for H_2O_3 are in good agreement with experiment. Reaction rate theory calculations are performed to assess the effect collisional stabilization of the vibrationally/rotationally excited intermediate H_2O_3* has on the apparent loss of the OH and HO_2 reactants. In the high-pressure limit each of the H_2O_3* intermediates is collisionally stabilized. However, at intermediate pressures the importance of collisional stabilization depends on the OH + HO_2 → H_2O_3 reaction exothermicity. The MP4 calculations reported here and a previous configuration interaction (CI) calculation place this exothermicity at −22 to −29 kcal/mol at 0 K. With use of these energies, the collisional stabilization of H_2O_3* at room temperature is predicted to become important only at pressures in excess of 5000 Torr for the commonly used bath gas He. Thus, at atmospheric pressures of an inefficient bath gas like He, the loss of the OH and HO_2 reactants is predicted to occur only on the triplet potential energy surface.

I. Introduction

As a result of its importance in atmospheric and combustion chemistry, the reaction

$$OH + HO_2 \rightarrow H_2O + O_2 \qquad (1)$$

has commanded the interest of both theoretical[1-3] and experimental[4-11] kineticists. It is not known whether the reaction mechanism is direct or proceeds through an intermediate complex. Two particularly intriguing aspects of this reaction are its negative temperature dependence[10] and its possible pressure dependence.[4-11] Because of its important position in the study of radical–radical kinetics, reaction 1 has been referred to as "the Holy Grail Reaction".[11]

Reaction 1 is also of interest because of its close relationship to peroxy–peroxy radical reactions, the simplest of which is[12,13]

$$HO_2 + HO_2 \rightarrow H_2O_2 + O_2 \qquad (2)$$

This class of reactions plays an important role in the combustion and atmospheric oxidation of hydrocarbons. Self- and cross-reactions have been studied for the alkylperoxy radicals CH_3O_2 and $C_2H_5O_2$.[14-20] An understanding of the mechanism and kinetics of reaction 1 may be helpful in establishing the mechanism and kinetics for peroxy–peroxy radical reactions.

TABLE I: Pressure Dependence Observed for k_1 at 298 K

P, Torr	k_1, 10^{-11} cm^3/molecule s	ref
1–3	7.3–6.2	4–8
75	8.0–5.8	9
730	12.0 ± 4.0	9
1–1000	11.0 ± 3.0	10
2	$8.0^{+3.0}_{-2.0}$	11

A major uncertainty regarding reaction 1 is its pressure dependence. A list of values of k_1 determined versus pressure at 298 K is given in Table I. The earliest measurements listed in this table[4-9] indicate that the reaction rate decreases with a decrease in pressure. To explain this effect, it was suggested[9] that reaction 1 is a composite of the two microscopic mechanisms

$$OH + HO_2 \rightarrow H_2O + O_2 \qquad (1a)$$

$$OH + HO_2 \rightleftharpoons H_2O_3^* \rightarrow H_2O + O_2$$
$$\qquad\qquad\quad \downarrow$$
$$\qquad\qquad\quad H_2O_3 \qquad (1b)$$

The role of increased pressure (i.e., larger M) would be to vibrationally quench H_2O_3* and give rise to an apparent pressure enhancement of the reaction rate.[1] However, the magnitude of the pressure dependence of k_1 has been called into question by the most recent experiments of Keyser[10] and Schwab et al.[11]

Rather strong evidence for formation of the vibrationally/rotationally excited trioxide intermediate H_2O_3* comes from the isotopic labeling studies of Dransfeld and Wagner.[8] In reactions of ^{18}OH with $H^{16}O_2$ they observed a substantial amount of ^{16}OH, which is indicative of trioxide formation followed by dissociation

(1) Mozurkewich, M. *J. Phys. Chem.* **1986**, *90*, 2216.
(2) Jackels, C. F.; Phillips, D. H. *J. Chem. Phys.* **1986**, *84*, 5013.
(3) Toohey, D. W.; Anderson, J. G. *J. Phys. Chem.* **1989**, *93*, 1049.
(4) Thrush, B. A.; Wilkinson, J. P. T. *Chem. Phys. Lett.* **1981**, *81*, 1.
(5) Keyser, L. F. *J. Phys. Chem.* **1981**, *85*, 3667.
(6) Sridharan, U. C.; Qiu, L. X.; Kaufman, F. *J. Phys. Chem.* **1981**, *85*, 3361.
(7) Temps, F.; Wagner, H. G. Max-Planck-Institut Strömungsforschung, Berichte 18 A (1980); *Ber. Bunsen-Ges. Phys. Chem.* **1982**, *86*, 119.
(8) Dransfeld, P.; Wagner, H. G. *Z. Naturforsch.* **1987**, *42a*, 471.
(9) De More, W. B. *J. Phys. Chem.* **1982**, *86*, 121.
(10) Keyser, L. F. *J. Phys. Chem.* **1988**, *92*, 1193.
(11) Schwab, J. J.; Brune, W. H.; Anderson, J. G. *J. Phys. Chem.* **1989**, *93*, 1030.
(12) Lightfoot, P. D.; Veyret, B.; Lesclaux, R. *Chem. Phys. Lett.* **1988**, *150*, 120.
(13) Hippler, H.; Troe, J.; Willner, J. *J. Chem. Phys.* **1990**, *93*, 1755.
(14) Kurylo, M. J.; Dagaut, P.; Wallington, T. J.; Neuman, D. M. *Chem. Phys. Lett.* **1987**, *139*, 513.
(15) Dagaut, P.; Wallington, T. J.; Kurylo, M. J. *J. Phys. Chem.* **1988**, *92*, 3833.
(16) Dagaut, P.; Wallington, T. J.; Kurylo, M. J. *J. Phys. Chem.* **1988**, *92*, 3836.
(17) Jenkin, M. E.; Cox, R. A.; Hayman, G. D.; Whyte, L. J. *J. Chem. Soc., Faraday Trans. 2* **1988**, *84*, 913.
(18) Wallington, T. J.; Japar, S. M. *Chem. Phys. Lett.* **1990**, *167*, 513.
(19) Lightfoot, P. D.; Veyret, B.; Lesclaux, R. *J. Phys. Chem.* **1990**, *94*, 708.
(20) Lightfoot, P. D.; Lesclaux, R.; Veyret, B. *J. Phys. Chem.* **1990**, *94*, 700.

0022-3654/91/2095-6784$02.50/0

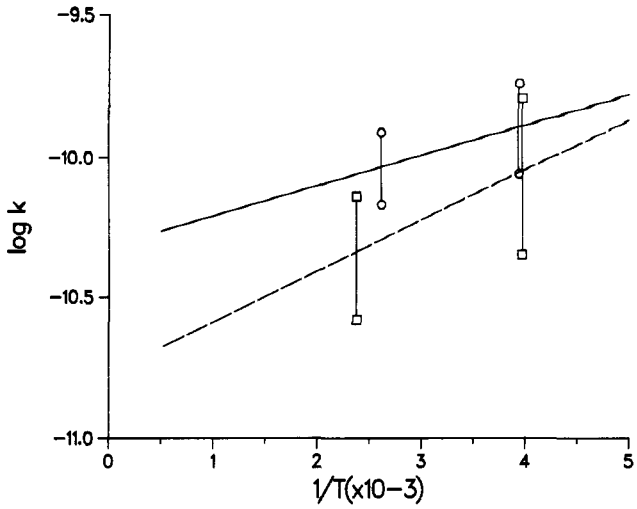

Figure 1. Predictions of k_1 (cm^3/molecule s) versus temperature for the 200–2000 K temperature range: solid curve, experimental result of ref 10 that $k_1 = 4.8 \times 10^{-11} \exp(250/T)$ for T = 254–382 K; dashed curve, experimental result of ref 22 that $k_1 = 1.7 \times 10^{-11} \exp(416/T)$ for T = 252–420 K. The error bars denote the uncertainties in the rate constants at the limits of the temperature ranges.

to the reactants. The amount of ^{16}OH they observed is consistent with similar OH + HO_2 bimolecular rate constants for reactions 1a and 1b. However, the isotopically labeled product $^{18}O^{16}O$ is not observed,[21] which is strong evidence that the excited trioxide does not dissociate to $H_2O + O_2$. Thus, the most recent experimental studies[8,10,11] indicate that the excited trioxide intermediate H_2O_3* is formed but that it neither dissociates to $H_2O + O_2$ nor is collisionally stabilized.

Though all experimental studies indicate that the rate of reaction 1 decreases with an increase in temperature, the exact form of the negative temperature dependence is unknown. In early work carried out at 2.5 Torr, Sridharan et al.[22] found that $k_1 = (1.7 \pm 0.5) \times 10^{-11} \exp[(416 \pm 86)/T]$ cm^3/molecule s over the 252–420 K temperature range. More recently, Keyser[10] reported that at 1 Torr $k_1 = (4.8 \pm 0.8) \times 10^{-11} \exp[(250 \pm 50)/T]$ cm^3/molecule s for T = 254–382. For illustration, these two measurements of k_1 are extended over the 200–2000 K temperature range in Figure 1.

One approach for calculating k_1 is to assume that the rate of reaction is controlled by the long-range attractive interaction between OH and HO_2.[11] This assumption gives rise to a capture model, for which reaction is assumed to occur when a critical separation between OH and HO_2 is attained.[23] The long-range interaction between OH and HO_2 is the dipole–dipole potential[24]

$$-(\mu_1\mu_2/R^3)[2 \cos\theta_1 \cos\theta_2 - \sin\theta_1 \sin\theta_2 \cos(\phi_1 - \phi_2)] \quad (3)$$

where μ_i is the absolute magnitude of the dipole moment and (θ_i, ϕ_i) refer to the spherical polar angles describing the orientation of r_i, with respect to the body-fixed axes, for molecule i. If the adiabatic approximation is made, so that quantum numbers for the reactant energy levels can be used to label adiabatic potential energy curves versus OH + HO_2 separation, the collision capture rate constant is found to be[25]

$$k(T) = 1.766p(T)(\pi/\mu)^{1/2}(\mu_1\mu_2)^{2/3}(k_BT)^{-1/6} \quad (4)$$

where μ is the reduced mass, k_B is the Boltzmann constant, and $p(T)$ is the probability of initiating the collision on the reaction surface. This latter term is given by[26]

$$p(T) = g^*/Q_e(T) \quad (5)$$

where g^* is the electronic degeneracy of the reaction surface and $Q_e(T)$ is the electronic partition function for the reactants. To apply this equation requires knowing on what potential energy surface (i.e., singlet or triplet) the reaction occurs.

Ab initio quantum chemical calculations[2,3,27] have provided insight into the mechanism for reaction 1. The potential energies and structures of different internal rotation conformations of the trioxide intermediate, H_2O_3, have been studied with Hartree–Fock theory using basis sets with and without polarization functions.[27] Electron correlation was treated via many-body perturbation theory. An important finding from this study are the large barriers for simultaneous rotation of both OH groups. Jackels and Phillips[2] performed an extensive study of the OH plus HO_2 potential energy surfaces using the SCF-CI method with basis sets of polarized double-ζ quality. They found that a hydrogen-bonded HO···HO_2 species has an electronic energy 4.7 kcal/mol below that of the reactants. The minimum energy geometry of the hydrogen-bonded species is planar, with triplet and singlet states, $^3A'$ and $^1A'$, that are essentially degenerate. The $^1A''$ and $^3A''$ hydrogen-bonded excited states, produced by rotation of the unpaired OH electron into the molecular plane, are found to be slightly bound. The reaction exothermicity for forming the H_2O_3 intermediate is found to be −22.2 kcal/mol at 0 K. This intermediate has C_2 symmetry and is in a ^1A electronic state. Both of the excited-state oxygen channels ($^1\Delta_g$ and $^1\Sigma_g^+$) could be correlated with the ^1A intermediate.[2] This is because the intermediate is nonplanar and lacks high symmetry, so that there is an absence of restrictions on the spatial symmetry of the intermediate. If the reaction is constrained to a planar configuration, only the $^3A''$ state has the correct symmetry for correlation with the ground-state triplet products $^3\Sigma_g^-(O_2)$ and $^1A_1(H_2O)$. Along a planar path, the $^3A'$ state is correlated with excited triplet channels. However, at large OH and HO_2 separations the $^3A'$ and $^3A''$ states are nearly degenerate, and extensive mixing of these states could arise from motions that distort the system away from planarity. As a result, it has been suggested that both the $^3A'$ and $^3A''$ state could lead to triplet products.[2]

Most recently, Toohey and Anderson[3] studied the triplet OH + HO_2 potential energy surfaces using HF and MP2 theory with 3-21G** and 6-31G** basis sets. From their calculation they found a saddlepoint for reaction 1a on the $^3A''$ potential energy surface. However, they concluded that this saddlepoint was not rate controlling and instead the rate constant for reaction 1a is determined by the long-range dipole–dipole interaction, i.e., eq 3. By comparing the energies of the OH + HO_2 reactants, the HO···HO_2 hydrogen-bonded species, and the $^3A''$ saddlepoint, they suggested that it might be possible for the reactive system to become temporarily trapped in the hydrogen-bonded form.

In recent research we have carried out extensive ab initio and rate calculations for reaction 1, with a goal of establishing the mechanism and kinetics for this reaction. One aspect of the research is to determine whether conventional theories like RRKM theory and transition-state theory[28] are applicable to this reaction or whether more sophisticated dynamical theories are required as has been suggested for other reactions.[29,30] In this paper we present our analysis of the kinetics on the singlet potential energy surface. Results for the triplet surface will be presented in a future paper.[31]

(21) Kurylo, M. J.; Klais, P.; Laufer, A. H. *J. Phys. Chem.* **1981**, *85*, 3674.
(22) Sridharan, U. C.; Qiu, L. X.; Kaufman, F. *J. Phys. Chem.* **1984**, *88*, 1281.
(23) Hase, W. L.; Wardlaw, D. M. In *Bimolecular Collisions*; Ashfold, M. N. R.; Baggot, J. E.; Royal Society of Chemistry: London, 1989; p 171.
(24) Hirschfelder, J. O.; Curtiss, C. F.; Bird, R. B. *Molecular Theory of Gases and Liquids*; Wiley: New York, 1954; p 27.
(25) Clary, D. C. *Mol. Phys.* **1984**, *53*, 3.
(26) Graff, M. M.; Wagner, A. F. *J. Chem. Phys.* **1990**, *92*, 2423.
(27) Cremer, D. *J. Chem. Phys.* **1978**, *69*, 4456.
(28) Steinfeld, J. I.; Francisco, J. S.; Hase, W. L. *Chemical Kinetics and Dynamics*; Prentice-Hall: Englewood Cliffs, NJ, 1989; Chapters 10 and 11.
(29) Bunker, D. L.; Hase, W. L. *J. Chem. Phys.* **1973**, *59*, 4621. Davis, M. J.; Skodje, R. T. In *Advances in Classical Trajectory Methods*; Hase, W. L., Ed.; JAI Press: Greenwich, CT; Vol. 1, Intramolecular and Nonlinear Dynamics, to be published.
(30) Vande Linde, S. R.; Hase, W. L. *J. Phys. Chem.* **1990**, *94*, 6148. Vande Linde, S. R.; Hase, W. L. *J. Chem. Phys.* **1990**, *93*, 7962.
(31) Gonzales, C.; Theisen, J.; Schlegel, H. B.; Hase, W. L.; Kaiser, E. W., work in progress.

TABLE II: Reactant and Product Geometries and Vibrational Frequencies[a]

	HF/6-31G**	MP2/6-31G**	expt[b]	ref[c]
		$OH_A + H_BO_2$ Reactants		
r_{OH_A}	0.955	0.971	0.970	36
r_{OH_B}	0.950	0.975	0.971, 0.977	37, 38
r_{OO}	1.309	1.325	1.331, 1.335	37, 38
θ	105.9	104.5	104.3, 104.1	37, 38
ω_{OH_A}	4052	3847	3738	36
ω_{OH_B}	4074	3713	3436	39
ω_{HOO}	1602	1460	1392	40
ω_{OO}	1252	1238	1098	41
		$^1O_2 + H_2O$ Products		
r_{OO}	1.166	1.274	1.216	42
r_{OH}	0.943	0.960	0.9572	43
θ	106.0	103.8	104.5	43
ω_{OO}	1998	1214	1509	42
$\omega_{OH,asym}$	4264	4033	3943	44
$\omega_{OH,sym}$	4147	3895	3832	44
ω_{HOH}	1770	1684	1648	44

[a] Bond lengths, angles, and vibrational frequencies are given in units of angstroms, degrees, and cm^{-1}, respectively. [b] The OH, O_2, and H_2O vibrational frequencies are harmonic values. For HO_2, fundamental anharmonic frequencies are listed. [c] The references refer to the experimental values.

TABLE III: Reactant and Product Absolute Energies[a]

method[b]	OH	HO_2	$O_2(^1\Delta)$	H_2O
HF	-75.388 33	-150.176 64	-149.533 00	-76.023 62
MP2	-75.534 38	-150.513 23	-149.904 52	-76.222 45
MP3	-75.544 16	-150.516 77	-149.882 23	-76.226 09
MP4	-75.547 57	-150.533 61	-149.915 42	-76.231 24
PHF	-75.390 69	-150.179 71		
PMP2	-75.533 57	-150.510 74		
PMP3	-75.544 96	-150.518 06		
PMP4	-75.548 37	-150.534 90		

[a] Energies are given in hartrees (1 hartree equals 627.51 kcal/mol). The HF energies are calculated at the HF geometries in Table II. The remaining energies are calculated at the MP2 geometries. The MP2 energy is full; the MP3, MP4, and all PMP*n* energies are frozen core. [b] The prefix P identifies a spin-projected calculation; see section II.A.

II. Ab Initio Calculations

A. Computational Methods. Ab initio molecular orbital calculations were performed using the GAUSSIAN 88 system of programs.[32] Fully optimized geometries, harmonic vibrational frequencies, and zero-point energy corrections for the reactants, intermediates, transition structures, and products involved in the reaction between HO_2 and OH (on the singlet surface) were calculated at the Hartree–Fock and MP2 levels using the 6-31G** basis set[32b] with analytical derivatives.[33]

Electron correlation was computed with fourth-order Moller–Plesset perturbation theory[34] in the space of single, double, triple, and quadruple excitations using the optimized geometries obtained at the Hartree–Fock and MP2 levels (MP4SDTQ/6-31G**//HF/6-31G** and MP4SDTQ/6-31G**//MP2/6-31G**, respectively). Since the energies of the reactants were calculated by unrestricted HF and MP*n* methods, an approximate spin projection method[35] was used to remove contamination from higher spin states (denoted by PMP*n* in Table III).

B. Geometries and Vibrational Frequencies for Reactants and Products. Ab initio and experimental[36-44] geometries and vibrational frequencies for the reactants and products are compared in Table II. Absolute energies calculated for the reactants and products are listed in Table III. The HF/6-31G** and MP2/6-31G** geometries for OH and HO_2 were presented previously by Toohey and Anderson.[3] However, in their work vibrational frequencies were only determined at the HF/6-31G** level of theory. The MP2 frequencies are seen to be in substantially better agreement with experiment than are the HF values. Ab initio POL-CI,[46] CI,[46] and contracted CI (CCI)[46] calculations have also been reported for the reactants. For OH the CI bond length and harmonic frequency are 0.970 Å and 3798 cm^{-1}, respectively, and are in excellent agreement with experiment. The CCI bond length is the same, but the OH stretch frequency is slightly larger, i.e., 3816 cm^{-1}.

To compare with the ab initio calculations, experimental harmonic vibrational frequencies are needed for HO_2. However, only anharmonic values have been reported, which are listed in Table II. As a guide for comparing ab initio and experimental HO_2 frequencies, an empirical correction[47] can be applied to the

TABLE IV: Structure and Vibrational Frequencies for the Trioxide Global Potential Energy Minimum[a]

coordinate[b]	HF/6-31G**	MP2/6-31G**
θ	80.8	78.7
R(OO)	1.373	1.441
R(OH)	0.949	0.972
α(OOO)	107.4	106.2
β(HOO)	103.5	100.2

MP2 Vibrational Frequencies

3796	O–H str	829 (755)	O–O str asym
3792	O–H str	537 (500)	OOO bend
1399	OOH bend	417	torsion
1395	OOH bend	366	torsion
904 (855)[c]	O–O str sym		

[a] Units are given in footnote *a* of Table II. [b] The coordinates are defined in ref 26 and Figure 2. θ is the H–OO–H dihedral angle. [c] Experimental frequencies[49] are given in parentheses.

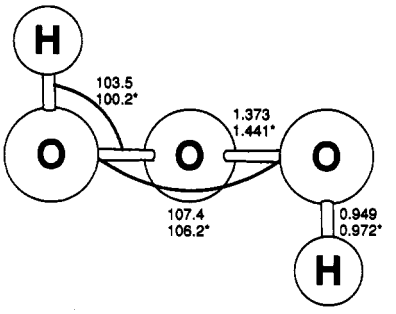

Figure 2. Calculated HF and MP2 (indicated by asterisks) geometries for the trioxide global minimum.

(32) (a) Frisch, M. J.; Head-Gordon, M.; Schlegel, H. B.; Raghavachari, K.; Binkley, J. S.; Gonzalex, C.; Defrees, D. J.; Fox, D. J.; Whiteside, R. A.; Seeger, R.; Melius, C. F.; Baker, J.; Martin, R.; Kahn, L. R.; Stewart, J. J. P.; Fluder, E. M.; Topiol, S.; Pople, J. A. GAUSSIAN 88; Gaussian Inc.: Pittsburgh, 1988. (b) Hariharan, P. C.; Pople, J. A. *Chem. Phys. Lett.* **1972**, *66*, 217.
(33) Schlegel, H. B. *J. Comput. Chem.* **1982**, *3*, 214.
(34) Defrees, D. J.; Raghavachari, K.; Schlegel, H. B.; Pople, J. A. *J. Am. Chem. Soc.* **1982**, *104*, 5576.
(35) Gonzales, C.; Sosa, C.; Schlegel, H. B. *J. Phys. Chem.* **1989**, *93*, 2435, and references therein.
(36) Walch, S. P.; Rohlfing, C. M.; Melius, C. F.; Bauschlicher Jr.; C. W. *J. Chem. Phys.* **1988**, *88*, 6273.
(37) Uehara, H.; Kawaguchi, K.; Hirota, E. *J. Chem. Phys.* **1985**, *83*, 5479.
(38) Beers, Y.; Howard, C. J. *J. Chem. Phys.* **1976**, *64*, 1541.
(39) Yamada, C.; Endo, Y.; Hirota, E. *J. Chem. Phys.* **1973**, *78*, 4379.
(40) Nagai, K.; Endo, Y.; Hirota, E. *J. Mol. Spectrosc.* **1981**, *89*, 520.
(41) Johns, J. W. C.; McKellar, A. R. W.; Riggin, M. *J. Chem. Phys.* **1978**, *68*, 3957. McKellar, A. R. W. *Faraday Discuss. Chem. Soc.* **1981**, *71*, 63.
(42) Herzberg, G. *Spectra of Diatomic Molecules*; Van Nostrand Reinhold: New York, 1950.
(43) Kern, C. W.; Karplus, M. *Water—A Comprehensive Treatise*; Franks, F., Ed.; Plenum: New York, 1972; Vol. 1, Chapter 2.
(44) Rosenberg, B. J.; Ermler, W. C.; Shavitt, I. *J. Chem. Phys.* **1976**, *65*, 4072.
(45) Dunning Jr., T. H.; Walch, S. P.; Goodgame, M. M. *J. Chem. Phys.* **1981**, *74*, 3482.
(46) Walch, S. P.; Rohlfing, C. M.; Melius, C. F.; Bauschlicher Jr., C. W. *J. Chem. Phys.* **1988**, *88*, 6273.
(47) A similar technique has been used successfully by spectroscopists to estimate the harmonic frequencies of methyl halides: Duncan, J. L.; McKean, D. C.; Speirs, G. K. *Mol. Phys.* **1972**, *24*, 553. Duncan, J. L.; Allan, A.; McKean, D. C. *Mol. Phys.* **1970**, *18*, 289.

TABLE V: Absolute Energies for the Global Minimum and Reaction Transition State[a]

method	global minimum	transition state
HF	-225.545 84	-225.445 77
MP2	-226.112 75	-226.031 54
MP3	-226.109 07	-226.015 49
MP4	-226.136 86	-226.060 28

[a] Energies are given in hartrees. The geometries for which these energies were determined are given in Tables IV and VII. The HF energy is for the HF geometry. The remaining energies were evaluated at the MP2 geometry (see footnote *a* in Table III).

anharmonic frequency to obtain an estimated harmonic frequency: ~5% higher for the OH stretch and ~1-2% higher for the HOO bend and OO stretch. With these corrections, the most significant difference between the MP2 and estimated harmonic vibrational frequencies is for the OO stretch. It is due in part to the difference between the MP2 and experimental OO bond length for HO_2. Both POL-CI[46] and CCI[46] calculations have been performed for HO_2. The POL-CI geometry and vibrational frequencies are r_{OH} = 0.991 Å, r_{OO} = 1.370 Å, θ = 103.3°, ω_{OH} = 3655 cm^{-1}, ω_{HOO} = 1457 cm^{-1}, and ω_{OO} = 1181 cm^{-1}. At the CCI level of theory, the geometry and vibrational frequencies for HO_2 are r_{OH} = 0.974 Å, r_{OO} = 1.334 Å, θ = 104.4°, ω_{OH} = 3531 cm^{-1}, ω_{HOO} = 1417 cm^{-1}, and ω_{OO} = 1220 cm^{-1}. The CCI results for HO_2 are in somewhat better agreement with experiment than are the results in Table II from the MP2 level of theory.

The MP2 geometry and vibrational frequencies for H_2O are in very good agreement with the experimental values. However, these MP2 results for H_2O are not as accurate as those obtained from higher order many-body perturbation theory and coupled cluster methods.[48] The experimental bond length and harmonic frequency for singlet O_2 are only approximately reproduced by either the HF or MP2 calculation. The large differences between the experimental and MP2 $^1O_2$ harmonic vibrational frequency and OO bond length are related. A MCSCF treatment is necessary for a more accurate determination of these properties for $^1\Delta_g(O_2)$.

C. Properties of the Trioxide Intermediate. In previous work, Cremer[27] performed an extensive ab initio study of the trioxide internal rotational potential energy surface. He determined energies and geometries for minima, local maxima, and saddlepoints on this surface. In the work presented here we have not attempted to perform a complete extension of the outstanding study by Cremer. Instead we have focused on the trioxide global minimum (Cremer's GMIN) and, during the course of the calculations, also considered one of the internal rotational saddlepoints (Cremer's S1). Our calculations for the trioxide potential energy surface employ the same level of theory as used by Cremer, i.e., HF and MP2, but incorporate the slightly larger 6-31G** basis set instead of the 6-31G* basis set used by Cremer.

In Table IV are listed the HF and MP2 geometries and vibrational frequencies found in this work for the trioxide global minimum GMIN. The HF and MP2 geometries are illustrated in Figure 2. A comparison with Cremer's[27] HF and MP2 geometries shows that all angles and bond lengths agree to within 0.6° and 0.008 Å, respectively. Apparently, the MP2 frequencies given in Table IV are the first ab initio values reported for the trioxide global minimum. The frequencies calculated for the bending and stretching modes of the oxygen framework are in very good agreement with the measured values (given in parentheses).[49] Absolute energies for GMIN are listed in Table V.

As discussed in section III.C, the properties of the H_2O_3 internal rotation transition states are not critical for the rate constant calculations reported here. Nevertheless, there is some general interest in these properties, and the geometry and vibrational frequencies found in this work for the S1 internal rotation transition state (Cremer's notation)[27] are given in Table VI. The

TABLE VI: Geometry and Vibrational Frequencies for the Trioxide S1 Internal Rotation Transition State[a]

coordinate[b]	HF/6-31G**	MP2/6-31G**
θ_1	-13.4	-14.7
θ_2	107.9	105.0
$R(O_1O_2)$	1.392	1.472
$R(O_2O_3)$	1.374	1.439
$R(O_1H)$	0.948	0.972
$R(O_3H)$	0.949	0.972
α(OOO)	107.1	105.2
$\beta_1(HO_1O_2)$	103.7	99.2
$\beta_2(HO_3O_2)$	103.1	99.7
absolute energies	-225.535 29	-226.102 83
HF Vibrational Frequencies		
	4124	1085
	4110	581
	1590	436
	1559	426*i*
	1182	

[a] Angles, bond lengths, absolute energies, and frequencies are in units of degrees, angstroms, hartrees, and cm^{-1}, respectively (see footnote *a* in Table III). [b] The coordinates and numbering scheme are defined in ref 26. θ_1 and θ_2 are the $H-O_1O_2-O_3$ and $H-O_3O_2-O_1$ dihedral angles, respectively.

TABLE VII: Geometry and Vibrational Frequencies for the Reaction Transition State

coordinate[a]	HF/6-31G**	MP2/6-31G**
θ_4	-1.8	-4.1
θ_5	-106.6	-97.0
$R(O_1O_2)$	1.406	1.337
$R(O_2O_3)$	1.479	1.712
$R(O_1H_4)$	1.469	1.309
$R(O_3H_5)$	0.954	0.981
α(OOO)	93.7	91.4
$\beta_1(H_4O_1O_2)$	71.7	77.9
$\beta_2(H_5O_3O_2)$	106.0	96.4

HF vibrational freq		MP2 vibrational freq	
4062	926	3714	744
2662	703	1894	536
1589	470	1383	305
1183	1101*i*	1344	2428*i*
971		863	

[a] The coordinates and numbering scheme are defined in ref 26 and Figure 3. θ_4 and θ_5 are the $H_4-O_1O_2-O_3$ and $H_5-O_3O_2-O_1$ dihedral angles, respectively.

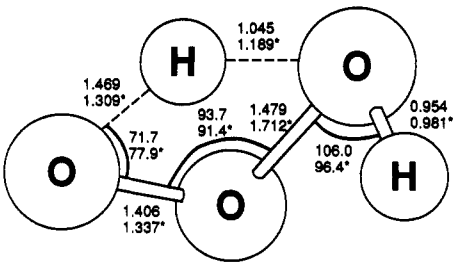

Figure 3. Calculated HF and MP2 (indicated by asterisks) geometries for the reaction transition state.

geometry found here using HF and MP2 theory with the 6-31G** basis set is nearly identical with that found by Cremer at the same level of theory but with the somewhat smaller 6-31G* basis set. The HF and MP2 relative energy between the S1 transition state and the global minimum GMIN are 6.62 and 6.23 kcal/mol, respectively. These values are only slightly smaller than the HF and MP2 S1 barrier heights of 6.8 and 6.5 kcal/mol reported by Cremer.[27]

D. $OH + HO_2 \rightarrow O_2(^1\Delta) + H_2O$ Transition State. A major emphasis of this study was to identify the transition state for

(48) Bartlett, R. J.; Schavitt, I.; Purvis III, G. D. *J. Chem. Phys.* **1979**, *71*, 281.
(49) Arnau, J. L.; Giguère, P. A. *J. Chem. Phys.* **1974**, *60*, 270.

TABLE VIII: Relative Electronic Energies for Stationary Points[a]

stationary pt	level of theory[b] HF	MP2	MP3	MP4
reactants	0.0	0.0	0.0	0.0
trioxide	15.41	-42.95	-28.89	-33.63
transition state	78.21	8.01	29.83	14.42
products	8.65	-51.87	-33.61	-39.78

[a] These are relative electronic energies in kcal/mol; i.e., zero-point energies are not included. The reactant energies used for determining these relative energies are the PHF, PMP2, PMP3, and PMP4 values in Table III. [b] The 6-31G** basis set was used (see footnote *a* in Table III).

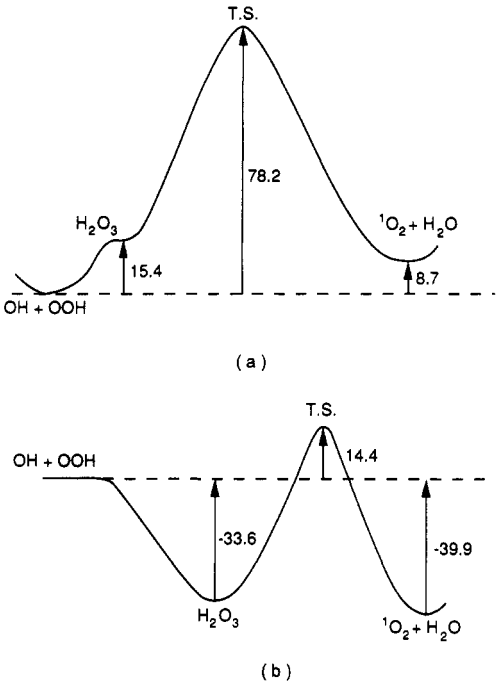

Figure 4. HF (a) and MP4 (b) reaction coordinate energies.

forming $O_2 + H_2O$ on the ^1A potential energy surface. The transition-state structure was optimized at both the HF and MP2 level and is shown in Figure 3. Specific values for the transition state's internal coordinates and its vibrational frequencies are listed in Table VII. An analysis of the occupied molecular orbitals for this ^1A transition state indicates that it correlates with the $^1\Sigma_g^+(O_2)$, $^1\Delta_g(O_2)$, and $^1A_1(H_2O)$ products.

Though the HF and MP2 geometries for the transition state are qualitatively the same, there are significant differences in the HF and MP2 values for some of the coordinates. In the MP2 transition state the rupturing OO bond, $R(O_2O_3)$, is much larger than in the HF transition state. The rupturing OH bond, $R(O_1H)$, is also longer in the MP2 than HF transition state. Consequently, there are also significant differences between the HF and MP2 vibrational frequencies for the transition state.

E. Reaction Energetics. Relative energies for the stationary points on the singlet potential energy surface are listed in Table VIII and depicted in Figure 4. These differences in electronic energies do not include the vibrational zero-point energies. One of the most profound aspects of these reaction energies is that HF theory incorrectly gives larger energies for the trioxide intermediate and products than the reactant energy. Even the qualitative shape of the HF potential energy curve is incorrect. This is perhaps not unexpected since a variety of bonds are formed and broken during the course of the reaction.

In previous calculations, Jackels and Phillips[2] found the electronic energy of the trioxide intermediate to be 26.4 kcal/mol lower than that of the reactants using the configuration interaction (CI) method with all single and double excitations and including Davidson's correction formula to account for quadruple excitations. A polarized double-ζ basis set was used in these calculations. The highest level of theory used here, MP4/6-31G**, gives a slightly lower electronic energy of 33.63 kcal/mol for the trioxide intermediate relative to reactants electronic energy. If the MP2 frequencies reported here for the reactants and trioxide intermediate (Tables II and IV) are used to calculate zero-point energies, the $OH + HO_2 \rightarrow H_2O_3$ 0 K reaction exothermicity is -21.9 kcal/mol from the calculation of Jackels and Philips and -29.09 kcal/mol from the MP4/6-31G** calculation reported here. The accuracy of this MP4 reaction exothermicity can be assessed by comparing experiment and theory for a related reaction. For $OH + HO \rightarrow H_2O_2$, experimental and MP4/6-31G* values for the 0 K reaction exothermicity are -49.6[50] and -43.4[51] kcal/mol, respectively. If a similar difference between experiment and MP4/6-31G** calculations exists for the $OH + HO_2 \rightarrow H_2O_3$ reaction, the calculations give an exothermicity 6 kcal/mol less negative than the experimental value. Higher level theory may be needed to establish a more accurate $OH + HO_2 \rightarrow H_2O_3$ reaction exothermicity. Hopefully, an accurate experimental value for this reaction exothermicity will become available in the near future.

TABLE IX: Low-Pressure Transition-State Theory Rate Constant for Reaction 1 on the Singlet Potential Energy Surface[a]

T, K	k, cm³/molecule s no tunnelling	tunnelling included[b]
200	2.01×10^{-30}	2.76×10^{-29}
300	4.19×10^{-25}	2.79×10^{-24}
500	8.50×10^{-21}	2.58×10^{-20}
750	1.53×10^{-18}	2.92×10^{-18}
1000	2.49×10^{-17}	3.76×10^{-17}
2000	3.31×10^{-15}	3.73×10^{-15}

[a] The rate constants were determined by using MP2 vibrational frequencies and geometries for the reactants and transition state and the MP4 potential energy barrier. [b] Tunnelling is included using the Wigner correction, eq 8.

The 0 K experimental heats of formation for OH, HO_2, $O_2(^1\Delta)$, and H_2O are 9.25,[52] 3.2,[53] 22.54,[42,52] and -57.10 kcal/mol,[52] respectively, which give a heat of reaction of -47.0 kcal/mol. In comparison, the MP4 heat of reaction at 0 K is -38.8 kcal/mol. To determine this energy, the MP2 frequencies were used to evaluate the reactant and product zero-point energies. A multireference configuration interaction calculation[45,46] may be needed to obtain better agreement with experiment.

III. Reaction Kinetics

A. $OH + HO_2 \rightarrow O_2(^1\Delta) + H_2O$. Under low-pressure conditions, so that the vibrationally/rotationally excited trioxide intermediate $H_2O_3^*$ is not collisionally stabilized, conventional transition-state theory[54] can be used to calculate the rate constant for reaction 1 on the singlet potential energy surface. The low-pressure conventional transition-state theory rate constant for reaction 1 on the singlet potential energy surface is given by

$$k = p(T)(k_B T/h) \exp(-\Delta G^{\ddagger}/RT) \qquad (6)$$

where $p(T)$ is the probability of initiating the collision on the singlet surface, and $\Delta G^{\ddagger}$ is the free energy difference between the transition state and reactants.

With use of eq 5, the appropriate expression for $p(T)$ can be deduced by considering the electronic energy levels of the reactants. Only the ground $^2A''$ electronic state of HO_2 is important, since the next electronic state $^2A'$ is 17 kcal/mol higher in energy.[55]

(50) Brouwer, L.; Cobos, C. J.; Troe, J.; Dübal, H.-R.; Crim, F. F. *J. Chem. Phys.* **1987**, *86*, 6171.
(51) Whitesick, R. A.; Frisch, M. J.; Pople, J. A. *Carnegie Mellon Quantum Chemistry Archive*; Carnegie Mellon University, 1983, and associated computer data base.
(52) *CRC Handbook of Chemistry and Physics*, 65th ed.; Weast, R. C., Ed.; CRC Press: Boca Raton, FL, 1984.
(53) Howard, C. J. *J. Am. Chem. Soc.* **1980**, *102*, 6937.
(54) Truhlar, D. G.; Hase, W. L.; Hynes, J. T. *J. Phys. Chem.* **1983**, *87*, 2664.
(55) Miller, J. A. *J. Chem. Phys.* **1981**, *74*, 5120.

TABLE X: Collision Capture Rate Constant for OH + HO_2 Association on the Singlet Surface

	k, 10^{-11} cm^3/molecule s		
T, K	vibrationally/rotationally adiabatic, eqs 4, 7	modified Langevin[55]	CVTST, eq 10
200	5.59	10.8	12.4
300	4.72	9.75	10.2
500	3.92	8.68	8.59
750	3.46		7.61
1000	3.20		7.05
2000	2.72		5.99

For OH($^2\Pi$) there are the two $^2\Pi_{1/2}$ and $^2\Pi_{3/2}$ spin–orbit states, which are separated by only 0.41 kcal/mol and are each doubly degenerate.[56] Combining these four OH spin–orbit states with the HO_2 $^2A''$ ground state gives rise to eight reactant electronic substates, four of which correlate with the $^1A'$ and $^3A'$ surfaces and four of which correlate with $^1A''$ and $^3A''$ surfaces. Inserting the above relative energies and electronic degeneracies into eq 5 gives the following expression for $p(T)$:

$$p(T) = 1/2[2 + 2\exp(-205/T)] \quad (7)$$

Tunnelling can be included by multiplying the rate constant by the Wigner correction factor

$$1 - \tfrac{1}{24}(h\nu^*/k_BT)^2 \quad (8)$$

where ν^* is the imaginary frequency at the transition state. In this paper, we use the MP2 geometries and vibrational frequencies for the reactants (Table II) and reaction transition state (Table VII) and the MP4 energy in Table VIII to solve eqs 6 and 8.

The rate constants calculated from eqs 6 and 7 with and without the tunnelling correction are listed in Table IX. A comparison of these rate constants with the experimental rate constants in Table I and Figure 1 shows that at only highly elevated temperatures is the formation of $^1O_2 + H_2O$ predicted to contribute significantly to the experimental reaction rate. Thus, these theoretical calculations are consistent with the experimental finding[21] that the reaction between ^{18}OH and $H^{16}O_2$ does not yield $^{18}O^{16}O$.

It is useful to consider how an error in the ab initio energy for the reaction transition state would affect the above rate constants. As discussed in section II.E, the MP4/6-31G** calculations underestimate the OH + $HO_2 \rightarrow {}^1O_2 + H_2O$ reaction exothermicity by 8 kcal/mol. If a similar error exists for the difference in energy between the reaction transition state and reactants, the calculated barrier for reaction is 8 kcal/mol too high. Lowering the barrier by this amount increases the rate constant by 5.5×10^8 at 200 K and 7.5 at 2000 K. However, these increases in the rate constant are not sufficient to make reaction on the singlet surface a significant contributor to the observed experimental rate.

B. OH + $HO_2 \rightarrow H_2O_3^*$ Association. The above analysis shows that the formation of oxygen and water is an unimportant process on the singlet potential energy surface, except at extremely high temperatures. However, loss of the OH and HO_2 reactants and apparent reaction could occur if the $H_2O_3^*$ vibrationally/rotationally excited intermediate is collisionally stabilized as shown in reaction 1b. As a first step to analyze the importance of this process, the rate constant for OH + $HO_2 \rightarrow H_2O_3^*$ association must be established.

In lieu of performing classical trajectory[57] or quantum[58] dynamical calculations, the rate constant for OH + HO_2 association on the singlet potential energy surface can be approximated by using a collision capture theory.[23] The capture rate constant used here is the one given by eq 4, which results from the vibrationally/rotationally adiabatic model of Clary.[25] The probability $p(T)$ of initiating the capture collision on the singlet surface is given by eq 7. The resulting singlet surface association rate constants are listed in Table X. Phillips[59] has developed a modified Langevin collision capture model and has applied it to OH + HO_2 association on the singlet surface by using the dipole–dipole potential in eq 3. The rate constants he determined are included in Table X. They are approximately 2 times larger than those found here by using eq 4.

Variational transition state theory (VTST)[23] can also be used to determine a capture rate constant for association. In microcanonical variation transition-state theory the transition state is located at the minimum in the number of states along the reaction path. The transition state is placed at the maximum in free energy along the reaction path in canonical variational transition state theory (CVTST). It is the latter version of transition state theory that is applied here. For these CVTST calculations it is assumed that neither the vibrational frequencies or geometries of OH and HO_2 vary along the association reaction path and that the distance between the OH and HO_2 centers of mass is the reaction coordinate value. If the OH + HO_2 interaction is assumed to be weak, the Hamiltonian for the degrees of freedom which vary along the reaction path can be written as a sum of terms that includes a "diatomic" rotation with a moment of inertia for the centers of mass of OH and HO_2, rotations of OH and HO_2 about their centers of mass, and the intermolecular potential between OH and HO_2, i.e.[60-62]

$$H = H_{2d,rot} + H_{OH,rot} + H_{HO_2,rot} + V(\theta_i,\phi_i) \quad (9)$$

If a classical partition function for the transition state is calculated from this Hamiltonian, the CVTST rate constant as a function of the reaction coordinate R^* is[58,59]

$$k(T,R^*) = p(T)\pi(R^*)^2(8k_BT/\pi\mu)^{1/2}\langle\exp[-V(\theta_i,\phi_i)/k_BT]\rangle \quad (10)$$

where the term in angular brackets represents a Monte Carlo average of $\exp[-V(\theta_i,\phi_i)/k_BT]$ over the θ_i,ϕ_i spherical polar angles of OH and HO_2. The CVTST rate constant for a particular temperature is the minimum in $k(T,R^*)$, which results from $(R^*)^2$ decreasing and the term in angular brackets increasing with a decrease in R^*.

To evaluate eq 10, we use the dipole–dipole potential in eq 3 for $V(\theta_i,\phi_i)$. The resulting CVTST rate constants for OH + $HO_2 \rightarrow H_2O_3^*$ association are listed in Table X. The value of R^* at the transition state is 4.9, 4.3, 3.6, 3.2, 2.9, and 2.3 Å, respectively, for T values of 200, 300, 500, 750, 1000 and 2000 K. Thus, as found for other association reactions,[23,60-64] the internuclear separation between the reactants at the transition state decreases as the temperature increases. The CVTST rate constants are approximately a factor of 2 larger than those resulting from the use of vibrationally/rotationally adiabatic theory, eq 4.

The more accurate VTST rate constant is given by microcanonical VTST.[65] The CVTST rate constant will be larger. An indication of the difference between the canonical and microcanonical rate constants for OH + $HO_2 \rightarrow H_2O_3^*$ can be attained from previous studies,[23] for which this difference ranges from 15–20% for $2CH_3 \rightarrow C_2H_6$ and 5–10% for H + $CH_3 \rightarrow CH_4$.[23] For the ion–molecule associations $Li^+ + H_2O \rightarrow Li^+(H_2O)$, $Li^+ + (CH_3)_2O \rightarrow Li^+[(CH_3)_2O]$, and $Cl^- + CH_3Cl \rightarrow Cl^-\cdots CH_3Cl$ the difference is somewhat larger and ranges from 20 to 55%.[23,31,64]

(56) Clary, D. C.; Werner, H.-J. *Chem. Phys. Lett.* **1984**, *112*, 346.
(57) See, for example: Swamy, K. N.; Hase, W. L. *J. Am. Chem. Soc.* **1984**, *106*, 4071. Duchovic, R. J.; Hase, W. L. *J. Chem. Phys.* **1985**, *82*, 3599.
(58) See, for example: Zhang, J. Z. H.; Miller, W. H. *J. Chem. Phys.* **1990**, *92*, 1811. Kress, J. D.; Bacic, Z.; Parker, G. A.; Pack, R. T. *Chem. Phys. Lett.* **1989**, *157*, 484. Yu, C.; Kouri, D. J.; Zhao, M.; Truhlar, D. G.; Schwenke, D. W. *Chem. Phys. Lett.* **1989**, *157*, 491.
(59) Phillips, L. F. *J. Phys. Chem.* **1990**, *94*, 7482.
(60) Wardlaw, D. M.; Marcus, R. A. *Chem. Phys. Lett.* **1984**, *110*, 230; *J. Chem. Phys.* **1985**, *83*, 3462; *J. Phys. Chem.* **1986**, *90*, 5383.
(61) Hase, W. L.; Duchovic, R. J. *J. Chem. Phys.* **1985**, *83*, 3448. Vande Linde, S. R.; Mondro, S. L.; Hase, W. L. *J. Chem. Phys.* **1987**, *86*, 1348. Hase, W. L.; Mondro, S. L.; Duchovic, R. J.; Hirst, D. M. *J. Am. Chem. Soc.* **1987**, *109*, 2916.
(62) Klippenstein, S. J.; Marcus, R. A. *J. Chem. Phys.* **1987**, *87*, 3410.
(63) LeBlanc, J. F.; Pacey, P. D. *J. Chem. Phys.* **1985**, *83*, 4511. Darvesh, K. V.; Boyd, R. J.; Pacey, P. D. *J. Phys. Chem.* **1989**, *93*, 4772.
(64) Aubanel, E. E.; Wardlaw, D. M. *J. Phys. Chem.* **1989**, *93*, 3117; *Chem. Phys. Lett.* **1990**, *167*, 145.
(65) Truhlar, D. G.; Garrett, B. C. *Acc. Chem. Res.* **1980**, *13*, 440.

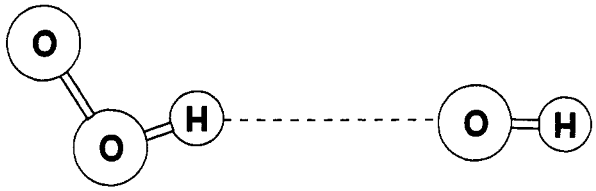

Figure 5. Model for the OH + HO_2 association transition state.

If a similar difference applies to the OH + HO_2 system, the microcanonical VTST rate constant will be larger than that from eq 4. Such a relationship is necessary, since a properly evaluated vibrationally/rotationally adiabatic rate constant will be less than or equal to that of microcanonical VTST.[66]

C. Pressure Dependence of H_2O_3 Formation. To study the effect of pressure on the loss of reactants, rate constants must be determined for the individual steps in reaction 1b, i.e.

$$OH + HO_2 \underset{k_{-1}}{\overset{k_1}{\rightleftharpoons}} H_2O_3^* \xrightarrow{k_2} H_2O + O_2$$
$$H_2O_3^* \xrightarrow{\omega} H_2O_3$$

On the basis of this mechanism, the RRKM/transition-state theory rate constant for the loss of either the OH or HO_2 reactant as a function of temperature and pressure (i.e., ω) is given by[67]

$$k(T,\omega) = \frac{\sigma p(T)}{hQ_{OH}Q_{HO_2}} \int_0^\infty dE \sum_{J=0}^{\infty} \frac{[\omega + k_2(E,J)]G^*_1(E,J)e^{-E/k_BT}}{\omega + k_{-1}(E,J) + k_2(E,J)} \quad (11)$$

where σ is the reaction path degeneracy, $p(T)$ is the electronic factor, Q_{OH} and Q_{HO_2} are the reactant partition functions, ω is the collision frequency, $G^*_1(E,J)$ is the sum of states at total energy E and angular momentum J for the transition-state separating reactants and $H_2O_3^*$, and $k_{-1}(E,J)$ and $k_2(E,J)$ are RRKM unimolecular rate constants versus E and J. Using a vibrator transition state model[68] and treating the K quantum number as active,[66,68-70] these unimolecular rate constants are given by the generic expression

$$k(E,J) = \sigma G^*(E,J)/hN(E,J) \quad (12)$$

where

$$G^*(E,J) = \sum_{K=-J}^{J} G^*[E - E_0 - E^*_r(J,K)] \quad (13a)$$

$$N(E,J) = \sum_{K=-J}^{J} N[E - E_r(J,K)] \quad (13b)$$

In these equations, $G^*(E,J)$ is the transition-state sum of states, $N(E,J)$ is the $H_2O_3^*$ density of states, E_0 is the unimolecular threshold, and $E^*_r(J,K)$ and $E_r(J,K)$ are the transition-state and $H_2O_3^*$ rotation energies. These energies are given by the "almost symmetric top" expression,[71] e.g.

$$E_r(J,K) = (I_a^{-1} + I_b^{-1})[J(J+1) - K^2]\hbar^2/4 + K^2\hbar^2/2I_c \quad (14)$$

The transition state for calculating $k_2(E,J)$ is located at the saddlepoint separating $H_2O_3^*$ and the $O_2(^1\Delta)$ + H_2O products and is given in Table VII. Since there is no saddlepoint separating OH + HO_2 and $H_2O_3^*$, microcanonical variational transition-state theory is the most accurate procedure to determine the transition state needed to evaluate the sum of states $G^*_1(E,J)$ and the unimolecular rate constant $k_{-1}(E,J)$.[72] An approximate variational transition-state theory approach is used here to determine these properties. The OH + HO_2 intermolecular potential is given by the dipole–dipole potential in eq 3 and the HO···HO_2 center-of-mass separation at the transition state is assumed to be the value determined from the CVTST calculation in the previous section. The dipole moments of OH and HO_2 are assumed to be aligned so that the transition state has the geometry given in Figure 5. (The ab initio CI Mulliken population[2] for HO_2 was used to determine the orientation of the HO_2 dipole moment.) It is also assumed that OH and HO_2 have the same geometries and vibrational frequencies in the transition state as for separated reactants. With these assumptions, all that is unknown about the transition state are its four intermolecular transitional mode[23] vibrational frequencies. These four frequencies were assumed to be degenerate, and their value was chosen by requiring the high-pressure limit of eq 11, $k(T,\omega\rightarrow\infty)$, to equal the vibrationally/rotationally adiabatic capture rate constant in Table X. The reactant MP2 geometries and vibrational frequencies given in Table II are used for this calculation. Parameters for the temperature dependent OH + $HO_2 \rightleftharpoons H_2O_3^*$ transition state are listed in Table XI.

TABLE XI: Parameters for the Model OH + $HO_2 \rightleftharpoons H_2O_3$ Transition State

parameter	temp, K 300	500	750	1000
R^*,[a] Å	4.3	3.6	3.2	2.9
E^*_0,[b] kcal/mol	−1.26	−2.15	−3.07	−4.12
I^*_i,[c] amu Å^2	224.2	162.1	131.6	111.1
	215.4	153.6	123.3	103.0
	8.71	8.48	8.28	8.09
ν^*_i,[d] cm^{-1}	79 (4)	104 (4)	125 (4)	145 (4)

[a] OH + HO_2 center-of-mass separation. [b] Classical potential energy difference between the transition state and reactants. Zero-point energies are not included. [c] Principal moments of inertia. [d] Vibrational frequencies for the transitional modes. The remaining vibrational frequencies for the transition state are the same as the OH and HO_2 reactant values.

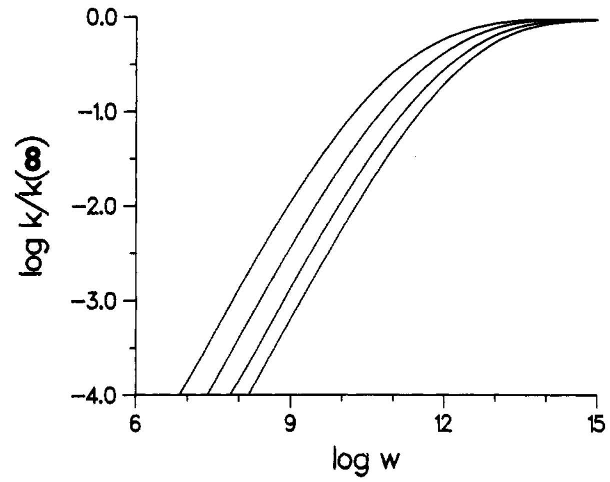

Figure 6. Plot of log $[k/k(\infty)]$ versus log ω for the potential surface with the MP4 OH + $HO_2 \rightarrow H_2O_3$ reaction exothermicity. The curves are for T = 300, 500, 750, and 1000 K. The upper curve is for T = 300 K and the lower curve for T = 1000 K.

As shown in Figure 5, OH and HO_2 do not have the proper relative orientation in the transition-state model used here for direct formation of $H_2O_3^*$. However, the OH and HO_2 moieties are highly flexible in the transition state. As a result, it is assumed that HO_2 can reorient to bring about H–O···O–O–H bond formation once the reactants move inside the transition state.

With use of these association transition states and the MP2 geometries and vibrational frequencies for the reactants (Table II), the H_2O_3 intermediate (Table IV), and the reaction transition

(66) Quack, M.; Troe, J. *Ber. Bunsen-Ges. Phys. Chem.* **1974**, *78*, 240.
(67) Gilbert, R. G.; Smith, S. C. *Theory of Unimolecular and Recombination Reactions*; Blackwell: Oxford, UK, 1990.
(68) Aubanel, E. E.; Wardlaw, D. M.; Zhu, L.; Hase, W. L. *Int. Rev. Phys. Chem.*, in press.
(69) Miller, W. H. *J. Am. Chem. Soc.* **1979**, *101*, 6810.
(70) Zhu, L.; Hase, W. L. *Chem. Phys. Lett.* **1990**, *175*, 117.
(71) Townes, C. H.; Schalow, A. L. *Microwave Spectroscopy*; McGraw-Hill: New York, 1955; pp 84–86.
(72) Hase, W. L. *Acc. Chem. Res.* **1983**, *16*, 258.

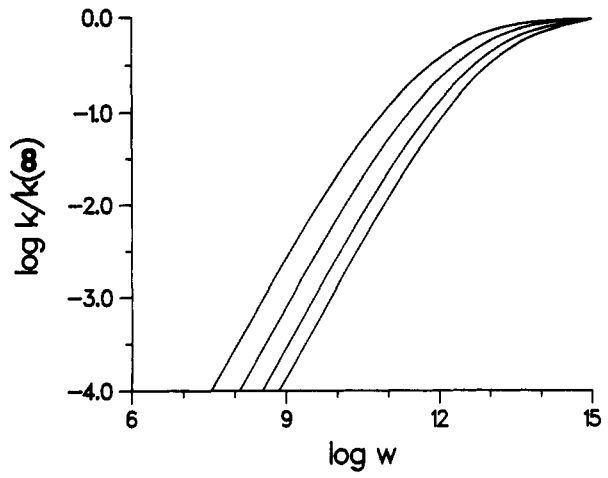

Figure 7. Plot of log $[k/k(\infty)]$ versus log ω for the potential surface with the CI OH + HO_2 → H_2O_3 reaction exothermicity. The curves are identified the same as in Figure 6.

state (Table VII), the rate constant in eq 11 was evaluated versus temperature and collision frequency. The first series of calculations were performed with the MP4 energies in Table VIII, which, after including zero-point energies, give a OH + HO_2 → H_2O_3 exothermicity of -29.09 kcal/mol and a threshold of 44.26 kcal/mol for H_2O_3 dissociation to $O_2(^1\Delta)$ + H_2O. The results of these calculations are given in Figure 6, where the logarithm of $k(T,\omega)/k(T,\omega\rightarrow\infty)$ is plotted versus the logarithm of ω for T = 300, 500, 750, and 1000 K. For the second series of calculations, the CI result[2] of 26.4 kcal/mol was used for the electronic energy difference between the reactants and trioxide intermediate. This energy, with zero-point energies included, gives a OH + HO_2 → H_2O_3 exothermicity of -21.9 kcal/mol and a H_2O_3 dissociation threshold for crossing the reaction transition state of 37.0 kcal/mol. Plots like those in Figure 6 are given in Figure 7 for these CI energetics. Comparing the results in Figures 6 and 7 shows that the MP4 H_2O_3 electronic binding energy gives a larger rate constant for OH (or HO_2) loss at a particular temperature and collision frequency than does the CI binding energy, because the lower CI H_2O_3 binding energy results in a larger unimolecular rate constant $k_{-1}(E,J)$.

The Lennard-Jones collision frequency[73] between H_2O_3* and the commonly used[7-11] bath gas helium is $\omega = 1.6 \times 10^7 P\ s^{-1}\ Torr^{-1}$ at 300 K, where P is the helium pressure in Torr. This collision frequency has an approximate $T^{-1/2}$ temperature dependence. An approximate frequency for the collision stabilization of H_2O_3* can be evaluated by multiplying ω by β the collision efficiency (i.e., $0 < \beta \leq 1$). Though β values used for helium are often lower than 0.1,[74] a rather conservative large value[73] of 0.25 is used for the analysis made here. Using this value for β, the 300 K curve in Figure 6, which results from the MP4 energetics, shows that $k/k(\infty)$ becomes greater than 0.1 for pressures in excess of 5000 Torr. Thus, at room temperature and for pressures near atmospheric (760 Torr), the MP4 energetics predict that the collisional stabilization of H_2O_3 in a helium bath will not contribute to the loss of OH and HO_2 on the singlet potential energy surface. From Figure 7 it is seen that the CI energetics require an even higher pressure of 20 000 Torr for $k/k(\infty)$ to equal 0.1 at room temperature.

Both Figures 6 and 7 show that for a fixed ω, H_2O_3* collisional stabilization becomes less important as the temperature is increased. These results in Figures 6 and 7 are in accord with the ^{18}OH + $H^{16}O_2$ isotopic labeling studies of Dransfeld and Wagner[8] performed at 2-9 Torr and room temperature. Under those conditions, our calculations show that essentially all of the isotopically labeled H_2O_3* should dissociate to yield nearly identical amounts of ^{16}OH and ^{18}OH.

IV. Summary

Both electronic structure and rate theory calculations have been used to study the reaction between OH and HO_2 on the singlet potential energy surface. Geometries and vibrational frequencies for stationary points on the potential energy surface are determined with the MP2/6-31G** level of theory. With these geometries, relative energies are determined with MP4/6-31G** calculations.

An important property of the singlet potential energy surface characterized in this work is the OH + HO_2 → $O_2(^1\Delta)$ + H_2O reaction transition state. With zero-point energies included, the MP4 calculation predicts this transition state to lie 15.2 kcal/mol higher in energy than the OH + HO_2 reactants. Thus, it is predicted that the formation of $O_2(^1\Delta)$ + H_2O is only an important process on the singlet surface at highly elevated temperatures in excess of 2000 K. This finding agrees with a previous experimental study.[8] The error in the MP4 value for the OH + HO_2 → $O_2(^1\Delta)$ + H_2O reaction exothermicity indicates that the MP4 barrier for reaction may be too large by as much as 8 kcal/mol. However, even if the barrier is lowered by this amount, reaction on the singlet surface still does not significantly contribute to the experimental reaction rate.

The H_2O_3 trioxide molecule is an intermediate on the singlet potential energy surface. Vibrational frequencies calculated for H_2O_3 at the MP2/6-31G** level of theory are in very good agreement with the experimental vibrational frequencies.[49] The OH + HO_2 → H_2O_3 reaction exothermicity has not been determined by experiment, and an attempt is made here to establish it by ab initio calculations. A previous CI calculation[2] gave -21.9 kcal/mol for this reaction exothermicity. The value found here from MP4/6-31G** calculations is -29.1 kcal/mol.

The model used here assumes that every OH + HO_2 capture collision on the singlet surface forms vibrationally/rotationally excited H_2O_3*. At high pressures, collisional stabilization of H_2O_3* will contribute to the rate of reaction 1 since the OH and HO_2 reactants will be consumed. At low pressures the singlet surface will not contribute to the rate of reaction 1, since all of the H_2O_3* will dissociate to reactants. The exact pressure dependence of H_2O_3* collisional stabilization is uncertain at this time, since the level of H_2O_3* excitation is unknown because of the uncertainty in the OH + HO_2 → H_2O_3 reaction exothermicity. However, neither the CI or MP4 value for the OH + HO_2 → H_2O_3 reaction exothermicity predicts significant collisional stabilization of H_2O_3* at room temperature and atmospheric pressure of helium, a commonly used bath gas. A 0 K reaction exothermicity substantially more negative than -30 kcal/mol is required for collisional stabilization of H_2O_3* at these conditions. A complete analysis of the pressure dependencies of H_2O_3 formation awaits an accurate determination of the OH + HO_2 → H_2O_3 reaction exothermicity by higher level theoretical calculations than those reported here and/or by experiment.

To establish, from the calculations reported here, the pressures at which collisional stabilization of H_2O_3* becomes important requires knowing the collision efficiency β. For collisions of He with H_2O_3* a relatively large value of 0.25 was used for β to obtain a lower bound to the pressures that yield significant collisional stabilization. Using a smaller value of β, which is often done,[74] would require higher He pressures for collisional stabilization. To determine a more precise relationship between H_2O_3* collision stabilization and the pressure of He or of any other bath gas will require more accurate collision efficiencies. A preferred (but difficult) approach for relating the probability to collisional stabilization to the pressure of a bath gas requires knowing energy-transfer probabilities and solving a master equation.[67]

To conclude, the results reported here indicate that the loss of HO and HO_2 by reaction on the single surface is insignificant except at very high pressures and/or temperatures. Thus, the reaction that has been observed experimentally at room temperature and pressures of 1-1000 Torr of He must be occurring on the triplet surface. To study this thesis in detail extensive ab

(73) Chan, S. C.; Rabinovitch, B. S.; Bryant, J. T.; Spicer, L. D.; Fujimoto, T.; Lin, Y. N.; Pavlou, S. P. *J. Phys. Chem.* **1970**, *74*, 3160.
(74) See, for example: Cobos, C. J.; Troe, J. *Z. Phys. Chem. (Munich)* **1990**, *169*, 129.

initio and reaction rate calculations are in progress for the triplet surface.[31] However, in lieu of the results from this study several observations still can be made. First, the model advanced by Phillips[59] to explain the OH + HO_2 kinetics assumes reaction on the singlet surface. Second, the OH + HO_2 adiabatic capture rate constants calculated here for the singlet surface (Table X) are smaller than the experimental rate constants (Table I). For the triplet surface, the adiabatic capture rate constants are a factor of 3 larger and in approximate agreement with the experimental rate constants.

Acknowledgment. This research was supported by the Ford Motor Corp. Scientific Research Laboratory and the Institute for Manufacturing Research at Wayne State University. These calculations were performed in part at the NSF Pittsburgh Supercomputing Center.

Anilinopyridinium: Solvent-Dependent Fluorescence by Intramolecular Charge Transfer

Heinz Ephardt and Peter Fromherz*

Abteilung Biophysik der Universität Ulm, D-7900 Ulm-Eselsberg, Germany *(Received: March 11, 1991)*

Considerable intramolecular charge transfer is induced in anilinopyridinium by electronic excitation and by twist of the central single bond. Polar solvents shift the absorption spectrum to the blue and the fluorescence spectrum to the red. The effect may be assigned to an enhanced reorganization energy as described by Marcus' formula for intermolecular electron transfer. The quantum yield of fluorescence is lowered by polar media. The effect may be assigned to a lowered energy barrier leading to a nonfluorescent twisted internal charge-transfer (TICT) state as described by a Kramers–Born formula that accounts for solvation and friction.

Introduction

Homologues of (aminostyryl)pyridinium with two and three conjugated double bonds are popular fluorescence indicators of fast voltage transients in neurons in culture and in brain.[1-3] The molecular mechanism of the voltage sensitivity of fluorescence is unknown. A model for a physical mechanism must be based on a photophysical characterization of the probes, of course. In a previous paper we studied the prototype of these styryl dyes—[(dibutylamino)styryl]pyridinium butanesulfonate.[4] Its fluorescence was found to be extremely sensitive to the polarity and viscosity of bulk solvents. We assigned this sensitivity to a modulation of radiationless deactivation that was not related to trans–cis photoisomerization. To confirm this interpretation we decided to study molecules without double bonds, i.e., to leave the class of styryl dyes and to consider anilinopyridinium dyes as presumable parent compounds of voltage-sensitive dyes. In this paper we present our results on (dibutylanilino)pyridinium butanesulfonate.

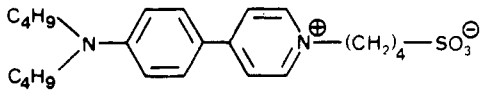

Computations

We computed the charge density of the positively charged chromophore of (dibutylanilino)pyridinium butanesulfonate. We applied the MNDO approximation[5] to the compound 1-methyl-4-(dimethylanilino)pyridinium using the program package MOPAC.[6]

We evaluated the charge distribution in the ground state and in the first excited state with limited configuration interaction (CI) as provided by MOPAC.[6] We varied the dihedral angle between pyridine and aniline, keeping the rest of the molecule at invariant geometry. A standard geometry was obtained by energy optimization of the ground state without CI imposing a set of symmetry conditions: The molecule, except for aliphatic hydrogens, had C_2 symmetry. The lengths of the aromatic CH bonds were equal. The methyl group at the pyridinium had C_{3v} symmetry. The angles of the CH bonds in the methylamino group were equal. The lengths of all aliphatic CH bonds were equal. (In the optimized structure the dihedral angle was 49°.) The distribution of net charge over the atoms and the atomic groups is shown in Figure 1 for the coplanar state and for the perpendicular state.

In the planar ground state three-quarters of the charge was found in the pyridinium. In the planar excited state two-thirds of the charge was found in the aniline: The polarity of the molecule was reversed by excitation, the two charge distributions being roughly mirror images of each other. In the perpendicular ground state 90% of the charge was found in the pyridinium, whereas in the perpendicular excited state 90% of the charge was found in the aniline. The reversal of polarity was enhanced by twist. A twisted internal charge transfer (TICT) occurs in the excited state[7-9] as related to the twist of the dieder angle between the aromatic rings. (Twist around the amine bond did not give rise to a significant change of the charge distribution.)

The pronounced rearrangement of charge in the processes of excitation and of twist suggests that polar solvents may give rise to a considerable modulation of the energy surfaces of ground state and excited state.

Materials and Methods

Synthesis. 4-(4-*N*,*N*-Dibutylanilino)pyridine was synthesized by palladium-catalyzed coupling of *p*-bromo-*N*,*N*-dibutylaniline and diethyl(4-pyridyl)borane referring to a general procedure for synthesis of arylpyridines.[10] The butylsulfonate group was introduced by butanesultone.[11] The product (dibutylanilino)-

(1) Cohen, L. B.; Lesher, S. In *Optical Methods in Cell Physiology*; deWeer, P., Salzberg, B. M., Eds.; Wiley: New York, 1986; p 71.
(2) Loew, L. M.; Simpson, L. L. *Biophys. J.* **1981**, *34*, 353.
(3) Grinvald, A.; Hildesheim, R.; Farber, I. D.; Anglister, L. *Biophys. J.* **1982**, *39*, 301.
(4) Ephardt, H.; Fromherz, P. *J. Phys. Chem.* **1989**, *93*, 7717.
(5) Dewar, M. J. S.; Thiel, W. *J. Am. Chem. Soc.* **1977**, *99*, 4899.
(6) Stewart, J. J. P. *MOPAC Manual*, 2nd ed.; University of Texas, Austin; *QCPE No. 455*.
(7) Grabowski, Z. R.; Rotkiewicz, K.; Siemiarczuk, A.; Cowley, J.; Baumann, W. *Nouv. J. Chim.* **1979**, *3*, 343.
(8) Rettig, W. *Angew. Chem.* **1986**, *98*, 969.
(9) Bonatic-Koutecky, V.; Koutecky, J.; Michl, J. *Angew. Chem.* **1987**, *99*, 216.
(10) Ishikura, M.; Ohta, T.; Terashima, M. *Chem. Pharm. Bull.* **1985**, *33*, 4755.

0022-3654/91/2095-6792$02.50/0